Medicine®

OBSERVATIONAL STUDY

OPEN

Reproducibility of Dynamic Contrast-Enhanced MRI in Renal Cell Carcinoma

A Prospective Analysis on Intra- and Interobserver and Scan–Rescan Performance of Pharmacokinetic Parameters

Haiyi Wang, MD, Zihua Su, PhD, Huiyi Ye, MD, Xiao Xu, PhD, Zhipeng Sun, MD, Lu Li, MD, Feixue Duan, MD, Yuanyuan Song, MD, Tryphon Lambrou, PhD, and Lin Ma, MD

Abstract: The objective of this study was to investigate the intra- and interobserver as well as scan–rescan reproducibility of quantitative parameters of renal cell carcinomas (RCCs) with dynamic contrast-enhanced magnetic resonance imaging (DCE-MRI).

A total of 21 patients with clear cell RCCs (17 men, 4 woman; age 37–69 years, mean age 54.6 years, mean size, 5.0 ± 2.2 cm) were prospectively recruited from September 2012 to November 2012. Patients underwent paired DCE-MRI studies on a 3.0 T MR system with an interval of 48 to 72 hours. The extended-Tofts model and population-based arterial input function were used to calculate kinetic parameters. Three observers defined the 2-dimensional whole-tumor region of interest at the slice with the maximum diameter of the RCC. Intraobserver and scan–rescan differences were assessed using paired *t* tests, whereas interobserver differences using two-way analysis of variance. Intra- and interobserver reproducibility and scan–rescan reproducibility were evaluated using within-subject coefficient of variation (wCoV) and intraclass correlation coefficient (ICC).

There were no significant intra-, interobserver, or scan–rescan differences in parameters (all $P > 0.05$). All ICCs for intra- and interobserver agreements were >0.75 ($P < 0.05$), whereas the scan–rescan agreement was moderate to good; V_e (0.764, 95% confidence interval [CI]: 0.378–0.925) and K_{ep} (0.906, 95% CI: 0.710–0.972) had higher ICC than K^{trans} (0.686; 95% CI: 0.212–0.898) and V_p (0.657; 95% CI: 0.164–0.888). In intra- and interobserver variability analyses, all parameters except V_p had low wCoV values. K^{trans} and V_e had slightly lower intraobserver wCoV (1.2% and 0.9%) compared with K_{ep} (3.7%), whereas all 3 of these parameters had similar interobserver wCoV values (2.5%, 3.1%, and 2.9%, respectively). Regarding scan–rescan variability, K^{trans} and K_{ep} showed slightly higher variation (15.6% and 15.4%) than V_e (10.1%). V_p had the largest wCoV in all variability analyses (all >30%).

DCE-MRI demonstrated good intra- and interobserver reproducibility and moderate to good scan–rescan performance in the assessment of RCC using K^{trans}, K_{ep}, and V_e as parameters under noncontinuous scanning mode. V_p showed poor reproducibility, and thus may not be suitable for this scanning protocol.

(*Medicine* 94(37):e1529)

Abbreviations: 3D = three-dimensional, AIF = arterial input function, CI = confidence level, DCE-MRI = dynamic contrast-enhanced magnetic resonance imaging, EES = extracellular extravascular space, ICC = intraclass correlation coefficient, wCoV = within-subject coefficient of variation, LAVA = liver acquisition with volume acceleration, MRI = magnetic resonance imaging, RCC = renal cell carcinoma, ROI = region of interest.

INTRODUCTION

Dynamic contrast-enhanced magnetic resonance imaging (DCE-MRI) has evolved from a tool for qualitative analysis, subjectively judging the enhancement of a target area on a visual basis and semiquantitative analysis/characterization of tumors using curvology,[1,2] to a fully quantitative tool for analyzing/evaluating parameters generated using pharmacokinetic models.[3,4] Through kinetic modeling of signal intensity changes resulting from the passage of contrast agent through the tumor vascular bed, DCE-MRI can produce physiologically related parameters, including the volume transfer constant from plasma to the extracellular extravascular space (EES) (K^{trans}), the efflux rate constant from EES back to plasma (K_{ep}), the ratio of the EES volume to tissue volume (V_e), and the ratio of blood plasma volume to tissue volume (V_p), which together may reflect tumor perfusion, vascular volume, and angiogenesis.

To date, pharmacokinetic parameters derived from DCE-MRI have been used extensively to evaluate tumor vessels, mainly reflecting 2 aspects: first, the characterization of benign versus malignant tumors[5] and the grading of malignant tumors,[6] and second, the evaluation of treatment effects, such as the therapeutic effects of molecularly targeted drugs[7] and chemotherapy.[8]

In renal tumors, DCE-MRI has played a key role in the delineation and characterization of masses, such as differentiating among RCC subtypes[9] and evaluating the therapeutic effects of molecularly targeted therapies.[10,11] Especially for the latter, pharmacokinetic parameters derived from quantitative DCE-MRI seem promising and may become surrogate

Editor: Giandomenico Roviello.
Received: June 17, 2015; revised: August 12, 2015; accepted: August 14, 2015.
From the Department of Radiology (HW, HY, LL, LM), Chinese PLA General Hospital, Beijing, China; Advanced Application (ZS), GE Healthcare, Beijing, China; Advanced Application (XX), GE Healthcare, Shanghai, China; Department of Radiology (ZS), Zhangjiakou First Hospital, Zhangjiakou City, Hebei Province, China; Medical Imaging Center (FD), Jiayuguan Jiugang Hospital, Jiayuguan City, Gansu Province, China; Department of Radiology (YS), General Hospital of Pingdingshan Coal Group, Pingdingshan City, Henan Province, China; and Lincoln School of Computer Science (TL), University of Lincon, Lincon, UK.
Correspondence: Lin Ma, Department of Radiology, Chinese PLA General Hospital, 28 Fuxing Road, Beijing 100853, China (e-mail: cjr.malin@vip.163.com).
The authors have no funding and conflicts of interest to disclose.
Supplemental Digital Content is available for this article.

ISSN: 0025-7974
DOI: 10.1097/MD.0000000000001529

biomarkers, which may be more convenient and accurate for monitoring dynamic changes in RCCs after receiving molecularly targeted drugs, potentially avoiding the need for repeated biopsies.

Because DCE-MRI showed potential in these areas, its reproducibility in quantitative analyses has drawn a lot of attention. To date, the methods and focus of DCE-MRI reproducibility studies have varied from assessing intra- and interobserver reproducibility to understanding scan–rescan reproducibility. However, for RCCs, the reproducibility of DCE-MRI in terms of pharmacokinetic analyses has not yet been thoroughly reported, in terms of observer or scan–rescan reproducibility.

In addition, conventional pharmacokinetic DCE-MRI has been performed using continuous scanning with high temporal resolution for pharmacokinetic analyses of target lesions. However, this sacrifices spatial resolution, and subsequently lowers the capacity of DCE-MRI sequence to cover a large scanning volume of interest. Furthermore, this method, in clinical practice, cannot meet the demands of high-quality DCE-MR images of abdominal organs, such as the liver and kidney, because of respiratory motion. Orton et al[12] reported the feasibility of obtaining functional liver perfusion estimates using a sequential breath-hold protocol. Thus, in the present study, in an attempt to balance the requirements of both clinical practice and pharmacokinetic analyses, we performed renal DCE-MRI as subjects held their breath, resulting in a noncontinuous scan mode. The aim of this study is to assess the intra- and interobserver as well as scan–rescan reproducibility of quantitative parameters of RCCs with noncontinuous DCE-MRI imaging.

MATERIALS AND METHODS

This prospective and observational study was approved by the local Institutional Review Board (Ethics Committee of Chinese PLA General Hospital). Written informed consents were obtained from all patients.

Patients

Patients with suspicious RCC during the computed tomography and ultrasound examinations were recruited at diagnosis from the urological clinic at our hospital between September 2012 and November 2012. To be included in this study, patients had to meet the following inclusion criteria: age $\geq$18 years old, glomerular filtration rate $>$60 mL/min, and size of lesions $>$1.0 cm in diameter to avoid partial volume artifact concerns, and clear cell RCCs—most common pathologic subtype. Exclusion criteria included common exclusion criteria for MRI scans and the use of Ga-related contrast, lesions with complete necrosis or cystic degeneration confirmed in MR examination and patients with poor DCE-MRI quality. Poor imaging quality should mainly meet the criteria—severe motion artifacts appeared in enhanced MRI and the images cannot be used for further evaluation.

Sample size estimation: sample size estimation for intraclass correlation coefficient (ICC) was performed using Power Analysis & Sample Size Software, PASS 11.0 (NCSS, LLC. Kaysville, UT). The preset condition included observers ($n = 3$), R_1 (expected ICC = 0.9), R_0 (acceptable lowest ICC = 0.75), $\alpha = 0.05$, and $\beta = 0.20$. At last the smallest sample size (k) was 19.

Procedure

MRI Technique

Patients underwent DCE-MRI twice: the first scan was within 48 hours of the initial diagnosis and the second scan was 48 to 72 hours after the first scan. MRI examinations were performed on a 3.0 T scanner (GE Discovery MR 750, GE Healthcare, Milwaukee, WI; maximum gradient strength 50 mT, maximum slew rate 200 mT/s) with an 8-channel surface phased-array coil. Patients practiced breathing techniques before each scan, which included breathing quickly during a nonscanning break and then breath-holding in the same position for as long as possible. Care was taken to ensure that, for each patient, rescanning was performed in the same lying position and the same anatomical location as the first scan. Routine clinical axial and coronal T2-weighted imaging was performed in all patients before dynamic studies to help localize and delineate tumors. The imaging protocol for DCE-MRI consisted of a precontrast T1 mapping sequence and a DCE sequence. The former included 5 consecutive axial 3-dimensional (3D) spoiled-gradient recalled-echo sequences for liver acquisition with volume acceleration (LAVA) with an array of flip angles (3°, 6°, 9°, 12°, and 15°) in breath-hold mode. Then, an axial DCE sequence (flip angle, 12°)—repeated scanning during 12 seconds of breath-holding for 2 phases and subsequently 6 seconds of breathing—was performed for 4.4 minutes to monitor contrast passage (Figure 1). Scanning parameters were as follows: repetition time 2.8 milliseconds, echo time 1.3 milliseconds, matrix 288 × 180, FOV 38 × 38 cm, slice thickness 6 mm, number of excitations 1, bandwidth 125 kHz, and parallel imaging acceleration factor 3. The contrast agent—Gadodiamide (0.1 mmol/kg, Omniscan, GE Healthcare)—was given intravenously when the second scan was started at a rate of 2 mL/s using a power injector (Spectris; MedRad, Warrendale, PA). The contrast bolus was flushed with 20 mL normal saline, administered at the same rate, to improve bolus coherence.

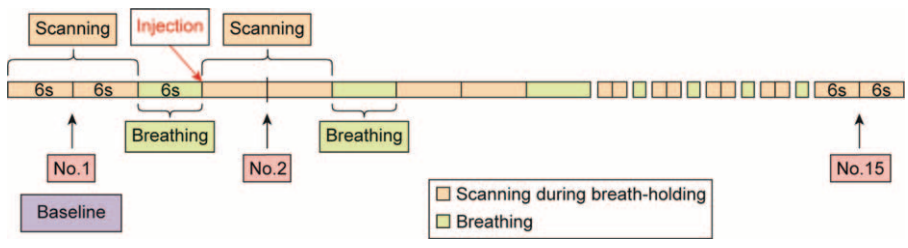

FIGURE 1. Dynamic contrast-enhanced MRI protocol. MRI scan was performed in a noncontinuous way—repeated scanning during 12 seconds breath-holding for 2 phases and subsequent 6 seconds breathing. The intravenous injection of MR contrast agent was started simultaneously when the second scanning session was initiated. MRI = magnetic resonance imaging.

Image Postprocessing and Analysis

All DCE-MRI analyses were conducted using open-source software packages, including the *R* package (http://dcemri.sourceforge.net/) and a medical image nonrigid registration package (http://cmictig.cs.ucl.ac.uk/wiki/index.php/NiftyReg).

All images were transferred to an Omni-Kinetics workstation (GE Healthcare, LifeScience, China) for analysis. Each patient's breath-holding position differed slightly and a soft organ as kidney changed its shape nonrigidly. Many articles have proposed using image registration methods[13] to handle body motion within time domain.[11,14] Here, the workstation provided an automatic nonlinear registration framework[15] to help remove any error of misalignment between consecutive MRI scans, thus making our results more accurate (for more visual results, please refer to Supplemental Digital Content, http://links.lww.com/MD/A431). The registration framework used a free-form deformation algorithm[16] as the main registration engine and mutual information as the correspondence metric.[17]

Data Collection

Calculation of Pharmacokinetic Parameters

The widely used 2-compartment extended-Tofts model[18] (Equation 1) with population-based arterial input function (AIF)[19] (Equation 2) was used to calculate parameters:

$$(1) \qquad C_t(t) = K^{\text{trans}} \int_0^t C_p(\tau) e^{\frac{K^{(trans)}}{V_e}(t-\tau)} d\tau + V_p \cdot C_p(t)$$

$$(2) \qquad C_p(t) = D(a_1 e^{-mt_1} + a_2 e^{-mt_2})$$

where in Equation 1, K^{trans} is the transfer constant from plasma to the EES; V_e is the ratio of the EES volume to tissue volume; V_p is the ratio of blood plasma volume to tissue volume; $K_{ep} = K^{\text{trans}}/V_e$ is the efflux rate constant from EES to plasma; and $C_p(t)$ and $C_e(t)$ are the contrast agent concentrations in the plasma and EES, respectively, and where in Equation 2, $D = 1.0$ mmol/kg, $a_1 = 2.4$ kg/L, $a_2 = 0.62$ kg/L, $m_1 = 3.0$ and $m_2 = 0.016$.[20]

Region of Interest Selection

Images were transferred to a Sun workstation (Sparc 10, Sun Microsystems, Mountain View, CA), where pharmacokinetic parameters were measured using the ImageJ software (National Institutes of Health, Bethesda, MD). Using reference information from anatomic axial and coronal T2-weighted images and postcontrast T1 images, 3 radiologists (ZS, FD, YS, all board-certified radiologists engaged in abdominal imaging for 8, 10, and 9 years, respectively) were instructed to place region of interests (ROIs) on the slice with the largest diameter of tumors on the dynamic images of DCE-MRI, covering the whole tumor where possible but excluding pulsatile artifacts from blood vessels and susceptibility artifacts from the adjacent bowels. Then, the same ROI was copied to all 4 parametric maps (K^{trans}, K_{ep}, V_e, and V_p) (Figure 2).

Because values of $K^{\text{trans}} > 1.2$ min^{-1} are commonly considered to represent errors because of measurement of pseudo-permeability in large blood vessels,[21,22] any pixels with $K^{\text{trans}} > 1.2$ min^{-1} or with V_e beyond the range of 0% to 100% were excluded from the parametric maps. Thus, we used the histogram function and set minimum and maximum values of K^{trans} (0, 1.2 min^{-1}), K_{ep} (0, 15 min^{-1}), V_e (0, 1), and V_p (0, 1); the mean values of K^{trans}, K_{ep}, V_e, and V_p were automatically calculated within the preset range.

Three observers (No. 1, ZS; No. 2, FD; and No. 3, YS) measured parameters of 2 DCE-MRI scans once, respectively, to examine interobserver and scan–rescan reproducibility. Then, the first observer (ZS) measured first scan again to evaluate intraobserver reproducibility.

Statistical Analyses

Intra-, Interobserver, and Scan–Rescan Differences in Pharmacokinetic Parameters

Intraobserver differences was assessed using paired *t* tests. Interobserver and scan–rescan differences were evaluated using two-way analysis of variance.

Variability Analyses

Intra-, interobserver, and scan–rescan variability of pharmacokinetic parameters were evaluated using the test–retest root-mean-square coefficient of variation method[23] to estimate the within-subject coefficient of variation (wCoV) of the whole study group for a pairwise comparison of all possible observer combinations. The wCoV (expressed as a percentage) is used to estimate variability by quantifying the variation in K^{trans}, K_{ep}, V_e, and V_p for a single individual from the study group for any pairwise comparison. Variability was considered acceptable when wCoV was within the goal of current quantitative imaging initiatives (Quantitative Imaging Biomarkers Alliance; coefficient of variation <20%).[24]

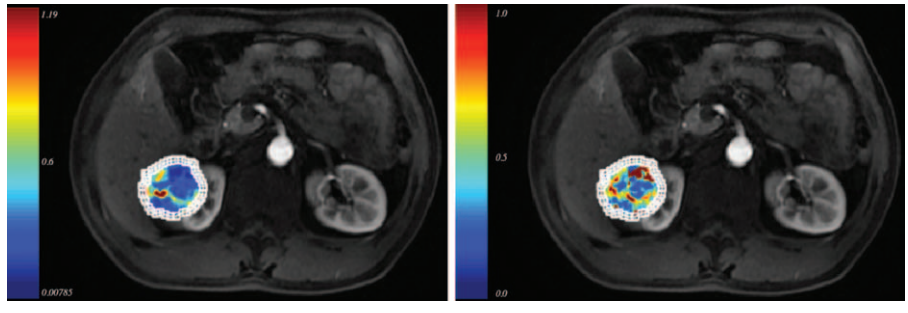

FIGURE 2. Graph showed placement of ROI on parametric maps of K^{trans} (A), and V_e (B) for renal cell carcinoma. K^{trans} = transfer constant from plasma to the extracellular extravascular space (EES), ROI = region of interest, V_e = the ratio of the EES volume to tissue volume.

TABLE 1. Kinetic Parameters and Comparison Between 2 Measurements for First MR Scan

Kinetic Parameters	First Measurement	Second Measurement	*P*
K^{trans} (min^{-1})	0.466 ± 0.142	0.466 ± 0.137	0.878
K_{ep} (min^{-1})	0.823 ± 0.353	0.834 ± 0.352	0.339
V_e	0.559 ± 0.107	0.558 ± 0.105	0.651
V_p ($\times 10^{-6}$)	2.299 ± 2.517	1.900 ± 1.832	0.473

MR = magnetic resonance.

Agreement Analyses

Intra-, interobserver, and scan–rescan agreements of pharmacokinetic parameters were evaluated using the ICC with a two-way mixed effect model. The agreement was defined as good (ICC > 0.75), moderate (ICC = 0.5–0.75), or poor (ICC < 0.5).

All statistical analyses were performed with the SAS software (ver. 9.3; SAS Institute Inc, Cary, NC) and GraphPad Prism (ver. 6.0; GraphPad Software, Inc, La Jolla, CA). *P* values <0.05 were considered to indicate a statistically significant difference.

RESULTS

Patients and Lesions Characteristics

A total of 28 patients with renal lesions underwent DCE-MRI scanning according to the given MR protocol. After the analysis of imaging quality and histopathology, 7 cases were excluded because of poor imaging quality (n = 2), papillary RCC (n = 1), chromophobic RCC (n = 3), and a benign renal angiomyolipoma lesion (n = 1). This resulted in 21 effective paired data sets of clear cell RCC cases (17 men, 4 woman; age 37–69 years, mean age 54.6 years, mean size, 5.0 ± 2.2 cm).

Pharmacokinetic Parameters of RCC

After setting the upper and lower limits for each kinetic value, the mean values of each pharmacokinetic parameter of each ROI were automatically calculated. They are listed in Tables 1 and 2.

Analysis of Differences in Kinetic Parameters

There were no statistically significant intra- or interobserver differences in any kinetic parameters examined (Tables 1), or between MRI scans (Table 3; all $P > 0.05$). The scan–rescan values measured by observer 1 for all of the parameters are presented in Figure 3.

Variability Analysis

For intraobserver variability, all parameters except V_p demonstrated low variation (Figure 4), where K^{trans} and V_e showed similar wCoVs (1.2% and 0.9%), lower than K_{ep} (3.7%). Variation in V_p was extreme (58%). For interobserver variability (Figure 5), K^{trans}, K_{ep}, and V_e showed similarly low wCoVs (2.5%, 3.1%, and 2.9%, respectively); V_p also demonstrated large variation (38%). In addition, each combination of comparison showed similar results to overall variability. Furthermore, scan–rescan variability (Figure 6) was greater than intra- and interobserver variability. K^{trans} and K_{ep} showed similar wCoVs (15.6%, 15.4%), and variation in K_{ep} was lowest (10.1%) and variation in V_p was highest (48%). In terms of both intraobserver and scan–rescan variability, V_e showed the lowest variation.

Agreement Analysis

The ICCs of all kinetic parameters in terms of both intra- and interobserver tests were all >0.75 and ICCs of K^{trans}, K_{ep}, and V_e were also >0.90, which are excellent agreements (range, 0.991–0.999; $P < 0.001$), with K^{trans} showing the highest intra- and interobserver ICC (0.999 and 0.993, respectively) (Table 4). However, in scan–rescan agreement analyses, the ICC of K_{ep} showed the highest value (0.906, 95% CI: 0.710–0.972, $P < 0.001$) followed by that of V_e (0.764 95% CI: 0.378–0.925, $P = 0.001$). K^{trans} and V_p demonstrated a moderate agreement with an ICC of 0.686 (95% CI: 0.212–0.898) and 0.657 (95% CI: 0.164–0.888), respectively (Table 4).

DISCUSSION

The reproducibility of pharmacokinetic parameters derived from DCE-MRI has been a controversial topic. Most studies have relied on scan comparisons obtained at 2 separate time points in the same patients without any intervening therapy.[22,23,25–29] Other studies simply assessed the within-subject variation in an identical DCE data set, making measurements at multiple times within and between observers.[30–33] A particular strength of our study is that it covers both aspects, and thus is a more comprehensive analysis of the reproducibility of pharmacokinetic parameters produced by DCE-MRI.

Previous studies have used different parameters for reproducibility analyses, depending on each study's aims. The most commonly used parameters have been K^{trans}, permeability surface (*PS*) product, and V_e, followed by K_{ep}; V_p is seldom used.

TABLE 2. Kinetic Parameters Measured by 3 Observers for First and Second MR Scan

	Observer 1		Observer 2		Observer 3	
Kinetic Parameters	**First Scan**	**Second Scan**	**First Scan**	**Second Scan**	**First Scan**	**Second Scan**
K^{trans} (min^{-1})	0.466 ± 0.142	0.450 ± 0.092	0.457 ± 0.132	0.443 ± 0.097	0.461 ± 0.137	0.456 ± 0.109
K_{ep} (min^{-1})	0.823 ± 0.353	0.760 ± 0.350	0.833 ± 0.358	0.711 ± 0.202	0.839 ± 0.368	0.707 ± 0.187
V_e	0.559 ± 0.107	0.560 ± 0.107	0.551 ± 0.116	0.592 ± 0.097	0.553 ± 0.118	0.569 ± 0.094
V_p ($\times 10^{-6}$)	2.299 ± 2.517	2.457 ± 4.027	2.337 ± 3.050	2.559 ± 3.240	2.498 ± 3.055	2.803 ± 3.948

MR = magnetic resonance.

TABLE 3. Interobserver and Scan–Rescan Comparison of Kinetic Parameters in Light of Two-Way ANOVA

	K^{trans}		K_{ep}		V_e		V_p	
Source	**F**	***P***	**F**	***P***	**F**	***P***	**F**	***P***
Observer	0.400	0.960	0.028	0.973	0.036	0.965	0.061	0.941
MRI scan	0.168	0.683	2.059	0.560	0.848	0.360	0.117	0.734
Observer* MRI scan	0.013	0.987	0.084	0.919	0.155	0.857	0.001	0.999

ANOVA = analysis of variance, MRI = magnetic resonance imaging.

K_{ep} is always larger than K^{trans} in value. In a range of studies on tumors, K_{ep} has been 2 to 5 times higher than K^{trans}, and V_e has ranged from 20% to 50%. In the present study, K_{ep} was 0.760 to 0.839 min^{-1}, nearly double the K^{trans} value of 0.450 to 0.466 min^{-1}, whereas V_e was 0.551 to 0.560, consistent with previous studies.[31,34] Our K^{trans} values were similar to those of a previous study[35] on pharmacokinetic parameters of RCC (0.51 ± 0.34 min^{-1}). However, our V_p value ($1.900–2.498 \times 10^{-6}$) was much smaller than in previous studies, which might have been influenced by the noncontinuous scanning mode that we used.

In the present study, K^{trans}, K_{ep}, and V_e showed low variation in both intraobserver (wCoV: 2.1%, 3.7%, and 0.9%, respectively) and interobserver (wCoV: 2.5%, 3.1%, and 2.9%, respectively) variability analyses. This is consistent with the results of some previous studies. Davenport et al[31] found that K^{trans}, K_{ep}, and V_e had similarly low variation (wCoV: 5.7%, 5.0%, and 3.9%, respectively) in assessments of uterine fibroids, and Beresford et al[30] reported 4.5%, 2.3%, and 1% wCoV in expert intraobserver analyses and 6.0%, 5.2%, and 2.7% wCoV in expert interobserver analyses, respectively, in assessments of breast cancer.

In the present study, intra- and interobserver agreements were excellent (all values >0.75). Similar results were reported by Davenport et al[31] (interobserver agreement: 0.88, 0.98, and 0.87 ICCs for K^{trans}, K_{ep}, and V_e, respectively) and Braunagel et al's[32] research on RCCs (ICC ranging from 0.79 to 0.97 for *PS*, V_e, and V_p in both intra- and interobserver agreement). However, unlike our results, Braunagel et al reported that *PS* was less reproducible than V_p, whereas V_e showed the lowest reproducibility (ICC = 0.6 and 0.64 in intra- and interobserver agreements), probably because of its insufficient scanning time (≤240 seconds). A previous study[36] showed that permeability parameters (K^{trans} or *PS* and V_e) are more dependent on total acquisition time than perfusion parameters (K_{ep}, V_p) and are sensitive to small differences in data with increasing variability.

Furthermore, regarding scan–rescan reproducibility, we found that K^{trans}, K_{ep}, and V_e had similar test–retest wCoV (15.6%, 15.4%, and 10.1%, respectively). Similar wCoV values

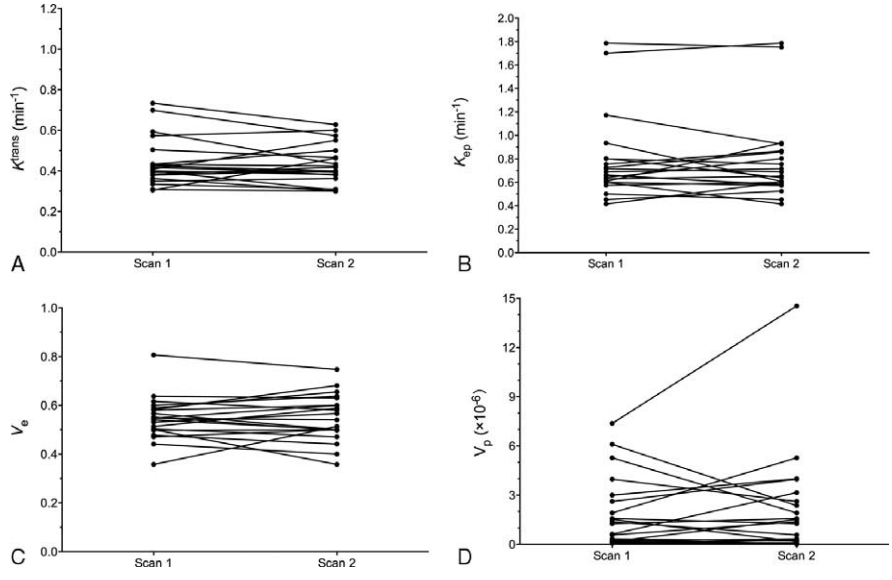

FIGURE 3. Graphs showed comparison of DCE-MRI kinetic parameters of 2 MRI scans of RCC for K^{trans} (A), K_{ep} (B), V_e (C), and V_p (D). DCE-MRI = dynamic contrast-enhanced magnetic resonance imaging, K^{trans} = transfer constant from plasma to the extracellular extravascular space (EES), K_{ep} = efflux rate constant from EES to plasma, MRI = magnetic resonance imaging, RCC = renal cell carcinomas, V_e = the ratio of the EES volume to tissue volume, V_p = the ratio of blood plasma volume to tissue volume.

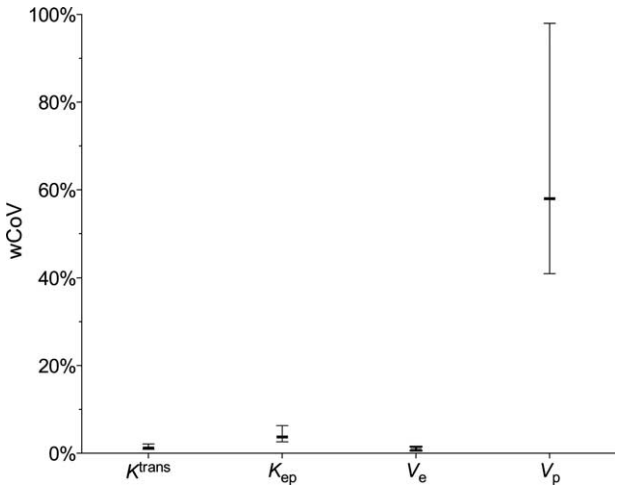

FIGURE 4. Graph showed intraobserver variability. Whereas K^{trans}, K_{ep}, and V_e showed similarly low variability, V_p showed highest variability (range of 41%–98 %). K^{trans} = transfer constant from plasma to the extracellular extravascular space (EES), K_{ep} = efflux rate constant from EES to plasma, V_e = the ratio of the EES volume to tissue volume, V_p = the ratio of blood plasma volume to tissue volume, wCoV = within-subject coefficient of variation.

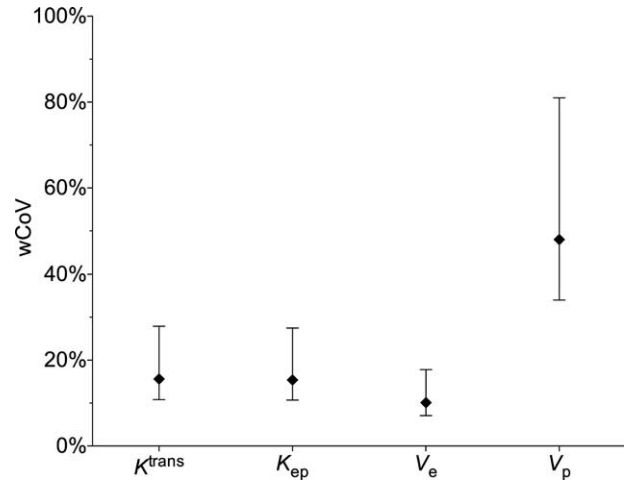

FIGURE 6. Graph showed scan–rescan variability. V_e showed lowest variation, whereas V_p showed highest variation. K^{trans} = transfer constant from plasma to the extracellular extravascular space (EES), K_{ep} = efflux rate constant from EES to plasma, V_e = the ratio of the EES volume to tissue volume, V_p = the ratio of blood plasma volume to tissue volume, wCoV = within-subject coefficient of variation.

for K^{trans} and V_e have been reported for abdominal tumors (19% and 14%) [23], and carotid atherosclerotic plaques (18% and 12%),[29] but higher than that of gliomas (7.7% and 6.2%),[22] which was probably because of inevitable motion of targeted abdominal organ, though imaging registration was used. In addition, the V_e values in the previous studies have been the most reproducible in test–retest analyses. Even in studies in which not all parameters have been acceptable, V_e has shown the lowest variation.[26,28]

However, in our study, the V_p value showed the largest variation among all parameters and across all analyses, probably because of the slow sampling method; nonetheless, this result is similar to or greater than the reported values regarding test–retest evaluations of carotid atherosclerotic plaque (40%)[29] and brain and abdominal tumors (39% and 30%, respectively).[23] For interscan agreement analysis, K_{ep} showed highest ICC (0.906). And V_e has higher ICC (0.764) than K^{trans} (0.686), which was in accordance with the previous studies in gliomas [22] and uterine fibroids.[24] Combined abovementioned variability with agreement analysis, K^{trans}, K_{ep}, and V_e were reproducible parameters in this noncontinuous DCE-MRI reproducibility studies.

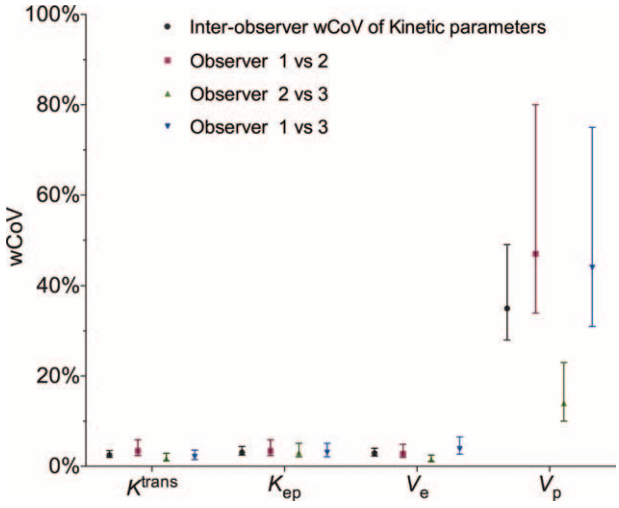

FIGURE 5. Graph showed interobserver variability for all possible observer combinations. K^{trans} = transfer constant from plasma to the extracellular extravascular space (EES), K_{ep} = efflux rate constant from EES to plasma, V_e = the ratio of the EES volume to tissue volume, V_p = the ratio of blood plasma volume to tissue volume, wCoV = within-subject coefficient of variation.

It should be noted that in our study scan–rescan reproducibility was lower than intra- and interobserver performance. Given proper training and guidance, interpersonal difference can be trivial. However, although image registration method was used, there is still accountable error introduced into dynamic images. Image registration can improve the accuracy of results but cannot totally fix the problem. Patients' hemodynamic information changes such as heart rate could also affect scan–rescan reproducibility.

In order to ensure the precision of DCE-MRI regarding the course of MRI scans, we made a great deal of efforts. Before scanning, we gave our technologists MRI scan training to ensure consistency in regards to parameters, the location plane between scans, and rules for measurements of pharmacokinetic parameters. We also gave patients respiratory training and advice on how to avoid discomfort. During scans, we used a series of 3D LAVA sequences, a type of spoiled-gradient echo-pulse sequence, which can markedly reduce the scanning time, especially for a large volume of interest (eg, whole kidneys), compared with 2D sequences, and still maintain a high signal-to-noise ratio. In addition, scanning as patients hold their breath can help alleviate the effects of respiratory motion. We set the breathing interval to 6 seconds, as short as possible. The noncontinuous scanning mode can lead to a low sampling rate; however, down sampling only slightly affects the fit quality at lower sampling resolution (6 and 24 seconds).[37]

TABLE 4. Intra-, Interobserver, and Scan–Rescan Agreement Analysis

	Intraobserver		Interobserver		Scan–Rescan	
Parameters	**ICC**	***P***	**ICC**	***P***	**ICC**	***P***
K^{trans}	0.999 (0.996, 1.000)	<0.001	0.993 (0.981, 0.998)	<0.001	0.686 (0.212, 0.898)	0.006
K_{ep}	0.993 (0.976, 0.998)	<0.001	0.993 (0.982, 0.998)	<0.001	0.906 (0.710, 0.972)	<0.001
V_e	0.998 (0.993, 0.999)	<0.001	0.991 (0.976, 0.997)	<0.001	0.764 (0.378, 0.925)	0.001
V_p	0.841 (0.538, 0.951)	<0.001	0.886 (0.732, 0.962)	<0.001	0.657 (0.164, 0.888)	0.007

ICC = intraclass correlation coefficient.

After MRI scanning, data processing was initiated. Before extracting pharmacokinetic parameters, we tested a published 3D nonrigid image registration method to correct misalignment caused by respiratory motion, which worked well and probably contributed to the near-ideal reproducibility values. During parameter extraction, the most sensitive method to a dynamic scan's temporal resolution is AIF. In noncontinuous scanning mode, it is almost impossible to have an identical AIF when performing scans twice in the same patient. This led us to use a population-based AIF method, rather than a personal AIF. This not only helped address temporal resolution difficulties, but also reduced AIF ROI location and sizing errors that have been reported previously.[38] The population-based AIF works equally well as the individual AIF for estimating pharmacokinetic parameters, as confirmed by several investigators.[39–41] Other reasonable alternatives for measuring DCE-MRI kinetics include a reference region model,[42] a double-reference model,[43] and a multiple-references model.[44] The advantage of these reference methods is that there is no requirement for direct AIF measurement. However, these models are not as widely used as the Tofts model, and are beyond the scope of this article.

Rules for ROI analysis using parametric maps have to be consistent and clearly defined. We chose ROIs covering the whole tumor at the slice with the maximum diameter instead of one or multiple smaller ROIs, based on a previous study[32] that concluded that the best interobserver and intraobserver correlations are obtained when a whole-tumor ROI is defined. In addition, in a previous study, the interobserver variability of K^{trans} was significantly lower in whole-lesion ROI analysis (10.6%) than in 3 out of 4 ROI analyses (20.1%) of uterine fibroids.[33]

This study has some limitations. First, the relatively low temporal resolution and short acquisition time might have led to inaccurate V_p values, in turn leading to large variation in reproducibility analyses. Second, we simply investigated 1 slice of tumors, which may not represent whole tumors. A 3D whole-tumor volume analysis with more pixels may reduce the variation in mean values of quantitative parameters and improve interobserver reproducibility compared with using slices, although a previous study[45] on primary RCC reported no significant differences in functional parameters in this respect. Thus, single-slice analysis may save time and workload. Third, because of necessity of image registration and establishment of kinetic parametric maps, the whole analysis process was relatively time-consuming, this is not ideal in real clinical practice, further more easily handled software or accelerating method should be investigated. Fourth, only clear cell RCC was enrolled in this study because clear cell RCC is the most common subtype and other subtypes were relatively less; it should be prudent that the result of this study is applied into other RCC subtypes because of biological difference of different tumors.

CONCLUSION

Our results indicate that DCE-MRI is a promising and reliable tool for pharmacokinetic analysis of RCC with good intra- and interobserver reproducibility and moderate to good scan–rescan performance using K^{trans}, K_{ep}, and V_e as parameters under a noncontinuous scanning mode. Further studies with a standardized scanning protocol are needed to ensure that results from various centers can be communicated conveniently and reliably.

ACKNOWLEDGMENTS

The authors would like to express their gratitude for the technical support and assistance from Zhenyu Zhou, PhD, and Dandan Zheng, PhD, of MR Research GE Healthcare China.

REFERENCES

1. El Khouli RH, Macura KJ, Jacobs MA, et al. Dynamic contrast-enhanced MRI of the breast: quantitative method for kinetic curve type assessment. *AJR Am J Roentgenol.* 2009;193:W295–300.
2. Engelbrecht MR, Huisman HJ, Laheij RJ, et al. Discrimination of prostate cancer from normal peripheral zone and central gland tissue by using dynamic contrast-enhanced MR imaging. *Radiology.* 2003;229:248–254.
3. Jackson A, O'Connor JP, Parker GJ, et al. Imaging tumor vascular heterogeneity and angiogenesis using dynamic contrast-enhanced magnetic resonance imaging. *Clin Cancer Res.* 2007;13:3449–3459.
4. Oostendorp M, Post MJ, Backes WH. Vessel growth and function: depiction with contrast-enhanced MR imaging. *Radiology.* 2009;251:317–335.
5. Bali MA, Metens T, Denolin V, et al. Tumoral and nontumoral pancreas: correlation between quantitative dynamic contrast-enhanced MR imaging and histopathologic parameters. *Radiology.* 2011;261:456–466.
6. Nguyen TB, Cron GO, Mercier JF, et al. Diagnostic accuracy of dynamic contrast-enhanced MR imaging using a phase-derived vascular input function in the preoperative grading of gliomas. *AJNR Am J Neuroradiol.* 2012;33:1539–1545.
7. Hsu CY, Shen YC, Yu CW, et al. Dynamic contrast-enhanced magnetic resonance imaging biomarkers predict survival and response in hepatocellular carcinoma patients treated with sorafenib and metronomic tegafur/uracil. *J Hepatol.* 2011;55:858–865.
8. Akisik MF, Sandrasegaran K, Bu G, et al. Pancreatic cancer: utility of dynamic contrast-enhanced MR imaging in assessment of antiangiogenic therapy. *Radiology.* 2010;256:441–449.
9. Sun MRM, Ngo L, Genega EM, et al. Renal cell carcinoma: dynamic contrast-enhanced MR imaging for differentiation of tumor subtypes—correlation with pathologic findings. *Radiology.* 2009;250:793–802.

10. Hahn OM, Yang C, Medved M, et al. Dynamic contrast-enhanced magnetic resonance imaging pharmacodynamic biomarker study of sorafenib in metastatic renal carcinoma. *J Clin Oncol.* 2008;26:4572–4578.
11. Rosen MA, Schnall MD. Dynamic contrast-enhanced magnetic resonance imaging for assessing tumor vascularity and vascular effects of targeted therapies in renal cell carcinoma. *Clin Cancer Res.* 2007;13 (2 pt 2):770s–776s.
12. Orton MR, Miyazaki K, Koh DM, et al. Optimizing functional parameter accuracy for breath-hold DCE-MRI of liver tumours. *Phys Med Biol.* 2009;54:2197–2215.
13. Ruthotto L, Hodneland E, Modersitzki J. Registration of dynamic contrast enhanced MRI with local rigidity constraint. In: Dawant B, Christensen G, Fitzpatrick JM, Rueckert D, eds. *Biomedical Image Registration. Vol. 7359.* Heidelberg: Springer Berlin; 2012:190–198.
14. Zollner FG, Sance R, Rogelj P, et al. Assessment of 3D DCE-MRI of the kidneys using non-rigid image registration and segmentation of voxel time courses. *Comput Med Imaging Graph.* 2009;33:171–181.
15. Klein A, Andersson J, Ardekani BA, et al. Evaluation of 14 nonlinear deformation algorithms applied to human brain MRI registration. *Neuroimage.* 2009;46:786–802.
16. Rueckert D, Sonoda LI, Hayes C, et al. Nonrigid registration using free-form deformations: application to breast MR images. *IEEE Trans Med Imaging.* 1999;18:712–721.
17. Pluim JP, Maintz JB, Viergever MA. Mutual-information-based registration of medical images: a survey. *IEEE Trans Med Imaging.* 2003;22:986–1004.
18. Tofts PS, Kermode AG. Measurement of the blood-brain barrier permeability and leakage space using dynamic MR imaging. 1. Fundamental concepts. *Magn Reson Med.* 1991;17:357–367.
19. Calamante F. Arterial input function in perfusion MRI: a comprehensive review. *Prog Nucl Magn Reson Spectrosc.* 2013;74:1–32.
20. Fritz-Hansen T, Rostrup E, Larsson HB, et al. Measurement of the arterial concentration of Gd-DTPA using MRI: a step toward quantitative perfusion imaging. *Magn Reson Med.* 1996;36:225–231.
21. Parker GJ, Suckling J, Tanner SF, et al. Probing tumor microvascularity by measurement, analysis and display of contrast agent uptake kinetics. *J Magn Reson Imaging.* 1997;7:564–574.
22. Jackson A, Jayson GC, Li KL, et al. Reproducibility of quantitative dynamic contrast-enhanced MRI in newly presenting glioma. *Br J Radiol.* 2003;76:153–162.
23. Roberts C, Issa B, Stone A, et al. Comparative study into the robustness of compartmental modeling and model-free analysis in DCE-MRI studies. *J Mag Reson Imaging.* 2006;23:554–563.
24. Heye T, Davenport MS, Horvath JJ, et al. Reproducibility of dynamic contrast-enhanced MR imaging. Part I. Perfusion characteristics in the female pelvis by using multiple computer-aided diagnosis perfusion analysis solutions. *Radiology.* 2013;266:801–811.
25. Padhani AR, Hayes C, Landau S, et al. Reproducibility of quantitative dynamic MRI of normal human tissues. *NMR Biomed.* 2002;15:143–153.
26. Galbraith SM, Lodge MA, Taylor NJ, et al. Reproducibility of dynamic contrast-enhanced MRI in human muscle and tumours: comparison of quantitative and semi-quantitative analysis. *NMR Biomed.* 2002;15:132–142.
27. Ferl GZ, Xu L, Friesenhahn M, et al. An automated method for nonparametric kinetic analysis of clinical DCE-MRI data: application to glioblastoma treated with bevacizumab. *Magn Reson Med.* 2010;63:1366–1375.
28. Lankester KJ, Taylor JN, Stirling JJ, et al. Dynamic MRI for imaging tumor microvasculature: comparison of susceptibility and relaxivity techniques in pelvic tumors. *J Magn Reson Imaging.* 2007;25:796–805.
29. Gaens ME, Backes WH, Rozel S, et al. Dynamic contrast-enhanced MR imaging of carotid atherosclerotic plaque: model selection, reproducibility, and validation. *Radiology.* 2013;266:271–279.
30. Beresford MJ, Padhani AR, Taylor NJ, et al. Inter- and intraobserver variability in the evaluation of dynamic breast cancer MRI. *J Magn Reson Imaging.* 2006;24:1316–1325.
31. Davenport MS, Heye T, Dale BM, et al. Inter- and intra-rater reproducibility of quantitative dynamic contrast enhanced MRI using TWIST perfusion data in a uterine fibroid model. *J Magn Reson Imaging.* 2013;38:329–335.
32. Braunagel M, Radler E, Ingrisch M, et al. Dynamic contrast-enhanced magnetic resonance imaging measurements in renal cell carcinoma: effect of region of interest size and positioning on interobserver and intraobserver variability. *Invest Radiol.* 2015;50:57–66.
33. Heye T, Merkle EM, Reiner CS, et al. Reproducibility of dynamic contrast-enhanced MR imaging. Part II. Comparison of intra- and interobserver variability with manual region of interest placement versus semiautomatic lesion segmentation and histogram analysis. *Radiology.* 2013;266:812–821.
34. Tofts PS, Brix G, Buckley DL, et al. Estimating kinetic parameters from dynamic contrast-enhanced T(1)-weighted MRI of a diffusable tracer: standardized quantities and symbols. *J Magn Reson Imaging.* 1999;10:223–232.
35. Chandarana H, Amarosa A, Huang WC, et al. High temporal resolution 3D gadolinium-enhanced dynamic MR imaging of renal tumors with pharmacokinetic modeling: preliminary observations. *J Magn Reson Imaging.* 2013;38:802–808.
36. Michaely HJ, Sourbron SP, Buettner C, et al. Temporal constraints in renal perfusion imaging with a 2-compartment model. *Invest Radiol.* 2008;43:120–128.
37. Lavini C. Simulating the effect of input errors on the accuracy of Tofts' pharmacokinetic model parameters. *Magn Reson Imaging.* 2015;33:222–235.
38. Cutajar M, Mendichovszky IA, Tofts PS, et al. The importance of AIF ROI selection in DCE-MRI renography: reproducibility and variability of renal perfusion and filtration. *Eur J Radiol.* 2010;74:e154–e160.
39. Wang Y, Huang W, Panicek DM, et al. Feasibility of using limited-population-based arterial input function for pharmacokinetic modeling of osteosarcoma dynamic contrast-enhanced MRI data. *Magn Reson Med.* 2008;59:1183–1189.
40. Parker GJ, Roberts C, Macdonald A, et al. Experimentally-derived functional form for a population-averaged high-temporal-resolution arterial input function for dynamic contrast-enhanced MRI. *Magn Reson Med.* 2006;56:993–1000.
41. Li X, Welch EB, Arlinghaus LR, et al. A novel AIF tracking method and comparison of DCE-MRI parameters using individual and population-based AIFs in human breast cancer. *Phys Med Biol.* 2011;56:5753–5769.
42. Lee J, Platt S, Kent M, et al. An analysis of the pharmacokinetic parameter ratios in DCE-MRI using the reference region model. *Magn Reson Imaging.* 2012;30:26–35.
43. Yang C, Karczmar GS, Medved M, et al. Estimating the arterial input function using two reference tissues in dynamic contrast-enhanced MRI studies: fundamental concepts and simulations. *Magn Reson Med.* 2004;52:1110–1117.
44. Yang C, Karczmar GS, Medved M, et al. Reproducibility assessment of a multiple reference tissue method for quantitative DCE-MRI analysis. *Magn Reson Med.* 2009;61:851–859.
45. Winter KS, Helck AD, Ingrisch M, et al. Dynamic contrast-enhanced magnetic resonance imaging assessment of kidney function and renal masses: single slice versus whole organ/tumor. *Invest Radiol.* 2014;49:720–727